Effects of Meteorology Changes on Inter-Annual Variations of Aerosol Optical Depth and Surface $PM_{2.5}$ in China—Implications for $PM_{2.5}$ Remote Sensing

Ling Qi [1], Haotian Zheng [2], Dian Ding [3], Dechao Ye [2] and Shuxiao Wang [2,4]

1 School of Energy and Environmental Engineering, University of Science and Technology Beijing, Beijing 100083, China

2 State Key Joint Laboratory of Environment Simulation and Pollution Control, School of Environment, Tsinghua University, Beijing 100084, China

3 Institute for Atmospheric and Earth System Research (INAR) /Physics, Faculty of Science, University of Helsinki, 00014 Helsinki, Finland

4 State Environmental Protection Key Laboratory of Sources and Control of Air Pollution Complex, Beijing 100084, China

Correspondence to: Shuxiao Wang (shxwang@tsinghua.edu.cn)

S1. Observations

In-Situ Station Radiometer AOD Measurements

We use AOD measurements from 16 in-situ sites (Figure S1 and Table S1) of the Sun-Sky Radiometer Observation Network (SONET, www.sonet.ac.cn) in 2012–2014. The sites are located in typical regions of China, including urban (Beijing, Shanghai, Zhoushan, Hefei, Nanjing, Chengdu, Xi'an and Harbin), desert (Minqin, Zhangye, and Kashi), coastal (Guangzhou, Sanya, and Haikou), basin (Chengdu), mountain (Songshan), and background plateau areas (Lhasa).

At SONET sites, AOD is measured by a multiwavelength polarized sun-sky radiometer CE318-DP manufactured by Cimel Electronique in France. The CE318-DP measures radiance and polorization of aerosol and water vapour at nine wavelengths: 340nm, 380nm, 440nm, 500nm, 675nm, 870nm, 936nm, 1020nm, and 1640nm. In this study, we use AOD measurements at 500nm. AOD-related products are prepared following version 2 protocols of AERONET at 3 levels [1]. AOD-related measurements are calibrated by a master instrument, which is regularly calibrated at AERONET/Photométrie pour le Traitement Opérationnel de Normalisation Satellitaire (PHOTONS) Izaña observatory by Langley plot approach with high precision [1]. Uncertainties of SONET AOD measurements stem from calibration, algorithm, and instrument performance. It is estimated that the uncertainty of SONET AOD measurements are similar as those of AERONET AOD observations [1], which is on the order of 0.01–0.02 [2]. The average AOD difference between SONET and AERONET is 0.002 ± 0.001, indicating comparable acquisition capability of SONET and AERONET measurements.

MODIS AOD Measurements

MODIS instruments are located on the Terra and Aqua satellites, launched into sun-synchronous polar orbits in December 1999 and May 2002, respectively (https://modis.gsfc.nasa.gov/). The MODIS instrument has one wide spectral range in 36 spectral bands from 0.41 μm to 14.5 μm, with spatial resolutions of 250 m (bands 1–2), 500 m (bands 3–7) and 1000 m (bands 8–36). Two global-coverage aerosol products are generated: the Level-2 daily product at 10-km and 3-km spatial resolution, and the Level-3 8-day, and daily products at a 1° longitude ×1° latitude resolution. We use MODIS Collection 6.1 Level-3 daily mean Dark Target and Deep Blue combined AOD data at 550 nm (https://modis-atmos.gsfc.nasa.gov/MOD08_M3/index.html). Compared to Collection 6, Collection 6.1 Dark Target Aerosol algorithm modified aerosol retrieval over land surface when urban percentage is larger than 20% using a revised surface characterization (Collection 6.1 Change Document). Deep Blue Aerosol algorithm improved surface modeling in elevated terrain and updated regional and seasonal aerosol optical models (Collection 6.1 Change Document). AERONET represents a BASE resource for the validation and bias-correction of satellite AOD datasets (Sayer et al., 2013 and references therein). The expected error for Dark Target retrievals at the 10-km spatial resolution is ± (0.05 + 15%) over land, indicating that about 66% of retrievals within the expected error on a global scale. The updated expected errors for Deep Blue retrievals are approximately ± (0.03 + 21%) for arid path retrievals and ± (0.03 + 18%) for vegetated path retrievals, respectively. On regional scale, the percentage of satellite data falling within the expected error might vary with regions. China shows a lower satellite retrieval accuracy compared to the other sites located in North Africa, Europe, and North America [3]. Bilal et al. showed that 60–83% of MODIS C6.1 AOD data were within range ± (0.05 + 15%) in NCP [4]. He et al. showed that 90% of MODIS C5 cases fall in the range of ± (0.05 + 20%) in YRD [5]. In addition, MODIS show a systematic negative bias when aerosol loadings are high.

Satellite retrieval of AOD is subject to uncertainties associated with radiometric calibration, assumption of aerosol properties, cloud contamination, and correction of the surface effect [6]. Cloud screening is one of the largest sources of discrepancies, especially on pixel and regional scales, but the uncertainty is difficult to quantify. The difference in the size distribution function

can create substantial AOD discrepancies of up to a factor of 2 [6]. Radiance calibration is a major source of uncertainty in AOD retrievals, changing AOD by more than 40% [6].

Surface In-Situ $PM_{2.5}$ Measurements

We use surface in-situ measurements of $PM_{2.5}$ from the China Ministry of Ecology and Environment network (CMEEN). In 2013, measurements at 670 sites are available in China, with 139 sites in NCP, 75 sites in YRD and 47 sites in PRD. From 2014 to 2017, site number of the monitoring network in China increased to 1498. 196 sites are in NCP, 107 sites are in YRD and 49 sites are in PRD. About 60% of the sites are using Thermo Scientific Continuous Ambient Particle Monitor TEOM-FDMS to measure $PM_{2.5}$ concentrations, and the rest are using an equivalent method β-gauge. $PM_{2.5}$ concentrations measured by the two methods are highly correlated (r^2 = 0.95), but the concentrations measured by TEOM equipment are 15~23% lower that those measured by β-gauge. Difference between β-gauge equipments is within 5% [7].

S2. Validation of AOD and Surface $PM_{2.5}$ Simulations

We validate MODIS observed and GEOS-Chem simulated AOD against SONET measurements at 16 in-situ stations (Figure S2 and Table S1). We use correlation coefficient (r) to validate the seasonal variations and root mean square error (RMSE) to quantify the discrepancies (Table S1). At Beijing and Songshan in NPC, MODIS observations agree well with SONET observations (r = 0.71 and 0.72; $RMSE/AOD_{SONET}$ = 24% and 20%). The latter show a single peak in summer, and the peak is largely from SNA as suggested by the model (Figure S3). In YRD, the seasonal variations of AOD are relatively flat, except at Shanghai, where AOD values fluctuate in summer. MODIS and GEOS-Chem perform the best at Zhoushan, where r values (MODIS: 0.92, model: 0.65) are larger than those at other sites and $RMSE/AOD_{SONET}$ (MODIS: 27%, model: 32%) are small. At Hefei and Nanjing, the correlation is relatively poor (r values for MODIS: 0.18 and 0.32, for GEOS-Chem: 0.15 and 0.07), and the discrepancies of MODIS (24% and 19%) are smaller than those of GEOS-Chem (both 39%) against SONET. At costal site Guangzhou in PRD, AOD has two peaks in spring and fall as observed by SONET. Both MODIS and GEOS-Chem underestimate annual mean AOD by 48%. The discrepancy is possibly attributed to the underestimate of sea salt along coast by the model.

GEOS-Chem reproduces the spatiotemporal variations of surface $PM_{2.5}$ with $RMSE/obs_{mean}$ of 0.27–0.42 and correlation coefficients of 0.57–0.71 (Figure S4). The normalized mean bias ((model-obs)/obs) and normalized mean error (|obs-model|/obs) of monthly $PM_{2.5}$ in NCP, YRD and PRD are -0.26–0.32 and 0.19–0.39. Negative bias is the largest in winter, when the model strongly underestimates $PM_{2.5}$ concentrations during pollution events. In addition, the model overestimate $PM_{2.5}$ concentrations in spring and summer due to the overestimate of [pNH_4^+] and [pNO_3^-]. We discuss detailed validation of $PM_{2.5}$ components and possible reasons for the overestimate in S3. Surface $PM_{2.5}$ concentrations are higher in winter and lower in summer in NCP, YRD and PRD, quite different from the seasonality of AOD in the three regions. Xu, J., et al. (2019) attributed the opposite seasonality of surface $PM_{2.5}$ and AOD in NCP to differences of aerosol vertical structures among seasons. They found that the high AOD in summer is mainly attributed to a strong enhancement of AOD in 500–1000m due to strong aerosol hygroscopic growth based on CALIOP observations. This enhancement accounts for 40% of the total column AOD.

Observations show that surface $PM_{2.5}$ is declining in 2013–2017 in all seasons in NCP (-5.7 – -13.3 μg m^{-3} yr^{-1}), YRD (-4.3 – -9.6 μg m^{-3} yr^{-1}) and PRD (-0.9 – -6.6 μg m^{-3} yr^{-1}, Figure S5). GEOS-Chem reproduces the declining trends in general, but underestimates the reduction rates in fall and winter by -19 – -77%. These strong underestimates are mainly attributed to the strong underestimate of $PM_{2.5}$ concentrations in 2013 and 2014, when pollution events were frequent and the model does not capture them.

GEOS-Chem (version 9.2) underestimates mean AOD observed by 24 AERONET sites in China by -40% in 2006–2009 but the correlation is strong: $r = 0.6$ for daily AOD and $r = 0.71$ for monthly AOD [8]. In addition, the model overestimates the contribution from SNA by ~20% across all regions, but underestimates the contribution from dust by ~10% [9]. They also found that the model shows poor performance for high AOD values due to the extremely high aerosol loadings. In this study, we use GEOS-Chem version 11.01, with improvements of BC scavenging [10], dust size distribution [11], brown carbon UV absorption [12] and acid uptake on dust aerosols [13]. The bias is now reduced to -21% compared to SONET observations at 16 sites. Compared to GOCART, GEOS-Chem shows a better performance in simulating the vertical profiles of AOD [14]. Thus, despite the negative biases, the state-of-art GEOS-Chem is still one of the best models to simulate aerosol distributions.

S3. Observed and Simulated Long-Term Trends of Aerosols in Key Regions

MODIS observations show negative trends of annual mean AOD in NCP, YRD, and PRD in 2006–2017, with statistical significant decreasing rates of -0.017, -0.016, and -0.016 yr^{-1} (-2.1, -2.1, and -3.1 % yr^{-1}), respectively ($p < 0.05$, Figure S6). The most important feature of these trends is that the reduction rates in 2013–2017 (NCP: -0.059 yr^{-1}; YRD: -0.037 yr^{-1}; PRD: -0.029 yr^{-1}) are 2–30 times of those in 2006–2013 (NCP: -0.002 yr^{-1}; YRD: -0.008 yr^{-1}; PRD: -0.013 yr^{-1}) in the three regions. AOD reduction rates in 2013–2017 are the largest ever-observed in China [15]. GEOS-Chem reproduces the MODIS observed 12-year mean AOD (within 15%) and the reduction rates (within 25%) in NCP, YRD and PRD in 2006–2017. The model also reproduces the inter-annual variations of annual mean AOD in the three regions ($0.75 < r < 0.89$) and the large differences of decreasing rates before and after 2013 (Figure S6). The simulated negative trends of AOD after 2013 are 9.4, 3.5 and 4.0 times of those before 2013 in NCP, YRD and PRD, respectively.

In-situ measurements show that annual mean surface $PM_{2.5}$ concentrations decrease at rates of -9.7, -6.2 and -3.9 μg m^{-3} yr^{-1} in NCP, YRD and PRD in 2013–2017 ($p < 0.05$, Figure S7). GEOS-Chem underestimates the negative trends by -30 – -44% in the three regions, possibly attributed to the underestimate of $PM_{2.5}$ concentrations during the frequent pollution events in 2013 and 2014. In addition, the reduction rates in 2013–2017 are 3.0, 2.0 and 2.2 times of those in 2006–2013 in NCP, YRD and PRD, respectively. In 2006–2017, annual mean surface $PM_{2.5}$ reduction rates are -2.6, -2.1 and -1.4 μg m^{-3} yr^{-1} (-3.4, -2.9 and -2.7 % yr^{-1}) in NCP, YRD and PRD, respectively (Figure S7).

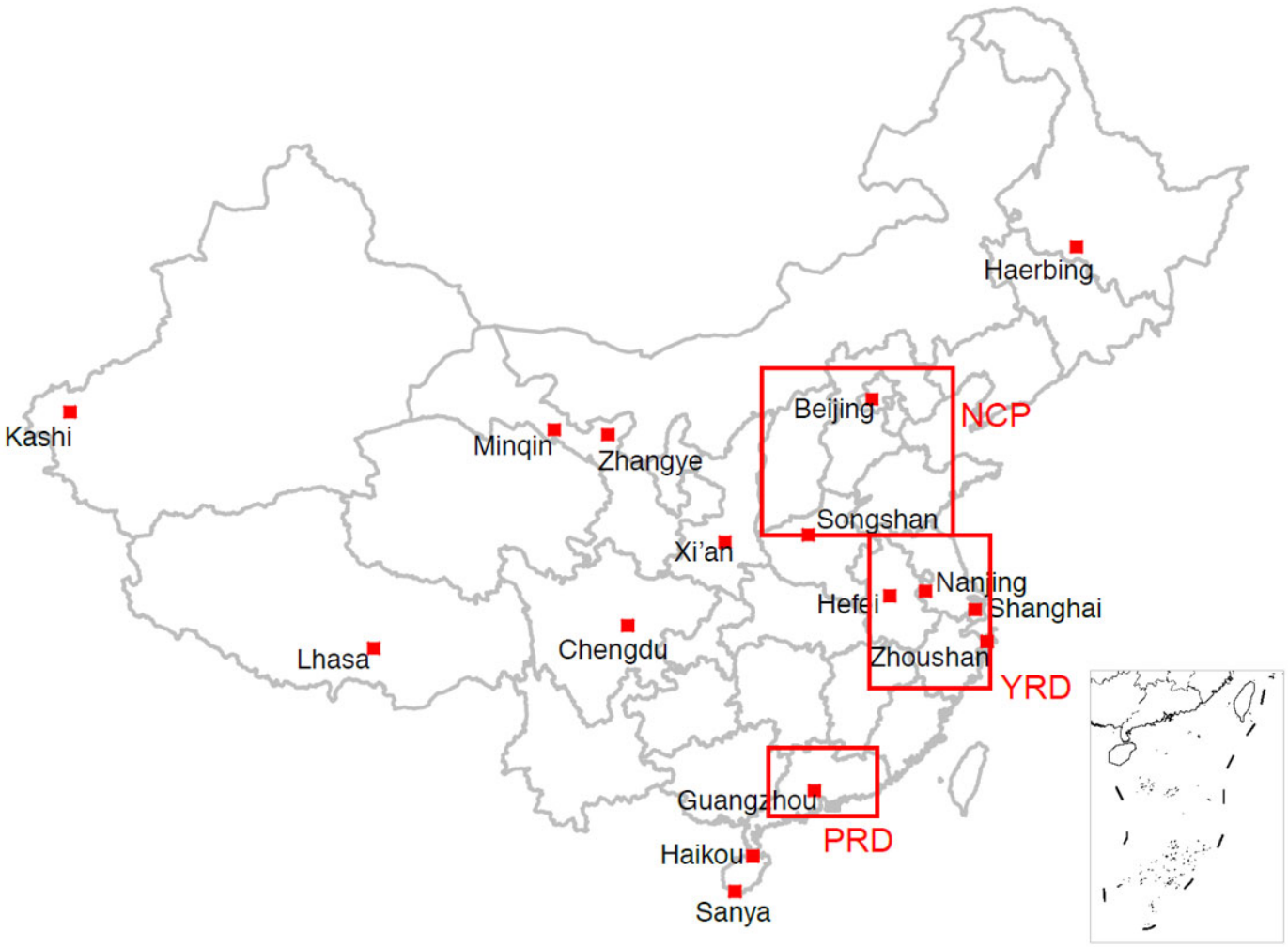

Figure S1: SONET sites and key regions in China: North China Plain (NCP, 35–41°N, 110–120°E), the Yangtze River Delta (YRD, 27–35°N, 116–122°E), and the Pearl River Delta (PRD, 22–25°N, 110–117°E).

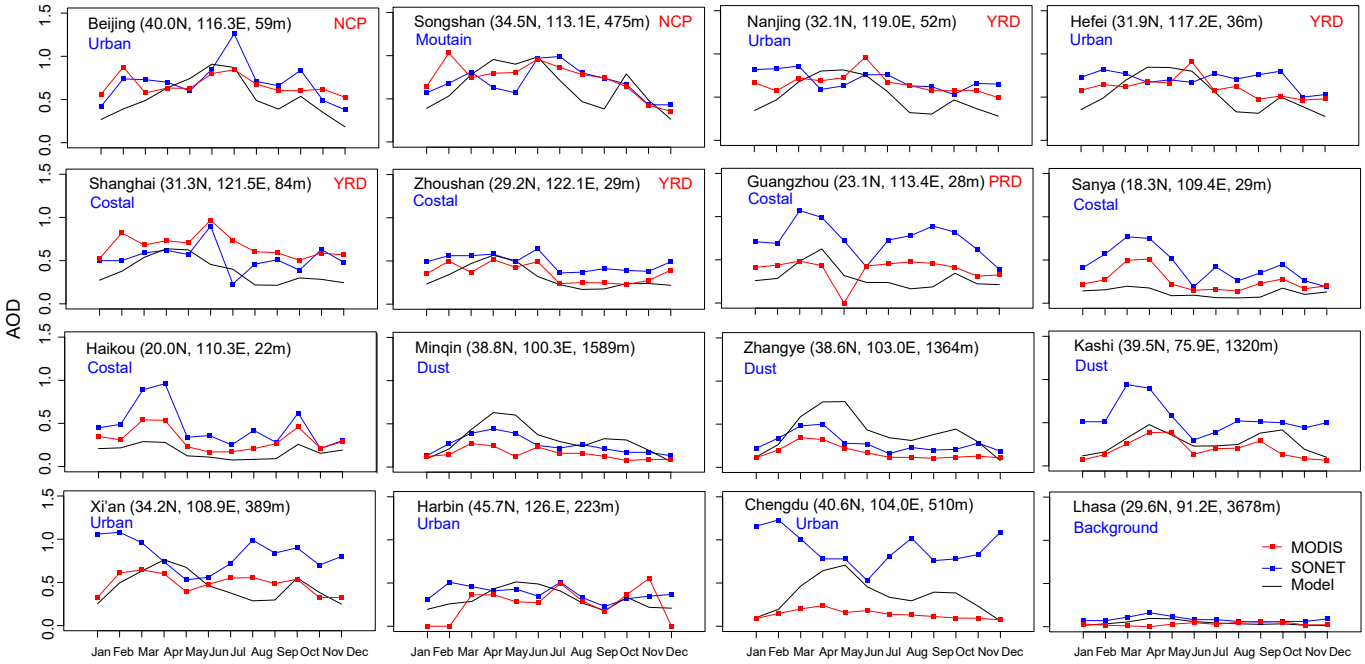

Figure S2: Monthly mean AOD from SONET (blue line) MODIS (red line) and GEOS-Chem (black line) averaged for 2013–2015. Beijing and Songshan are in the NCP region. Shanghai, Zhoushan, Nanjing and Hefei are in the YRD region. Guangzhou is in the PRD region.

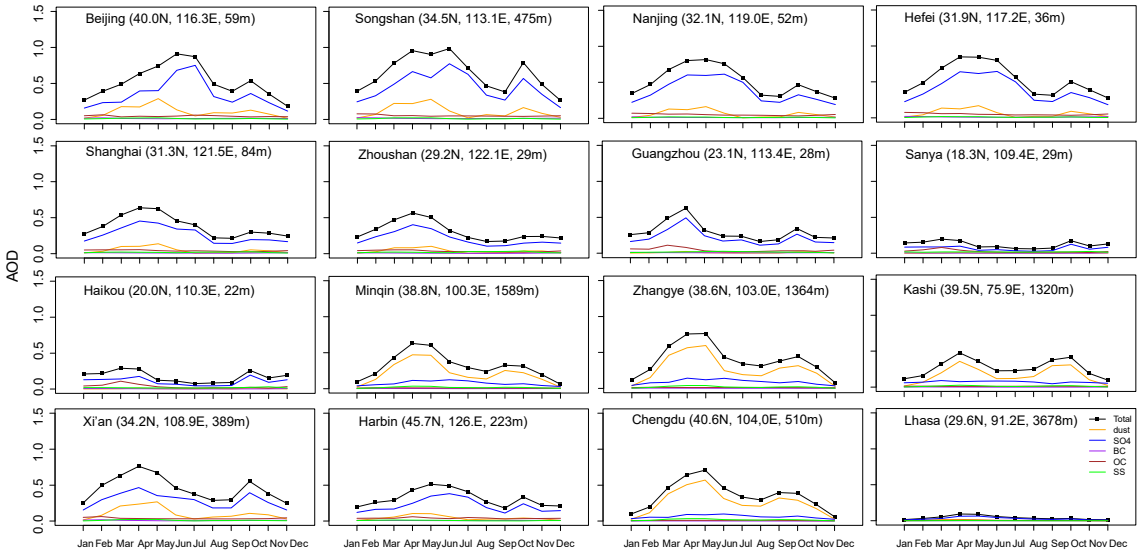

Figure S3: GEOS-Chem simulated monthly mean AOD components averaged for 2013–2015.

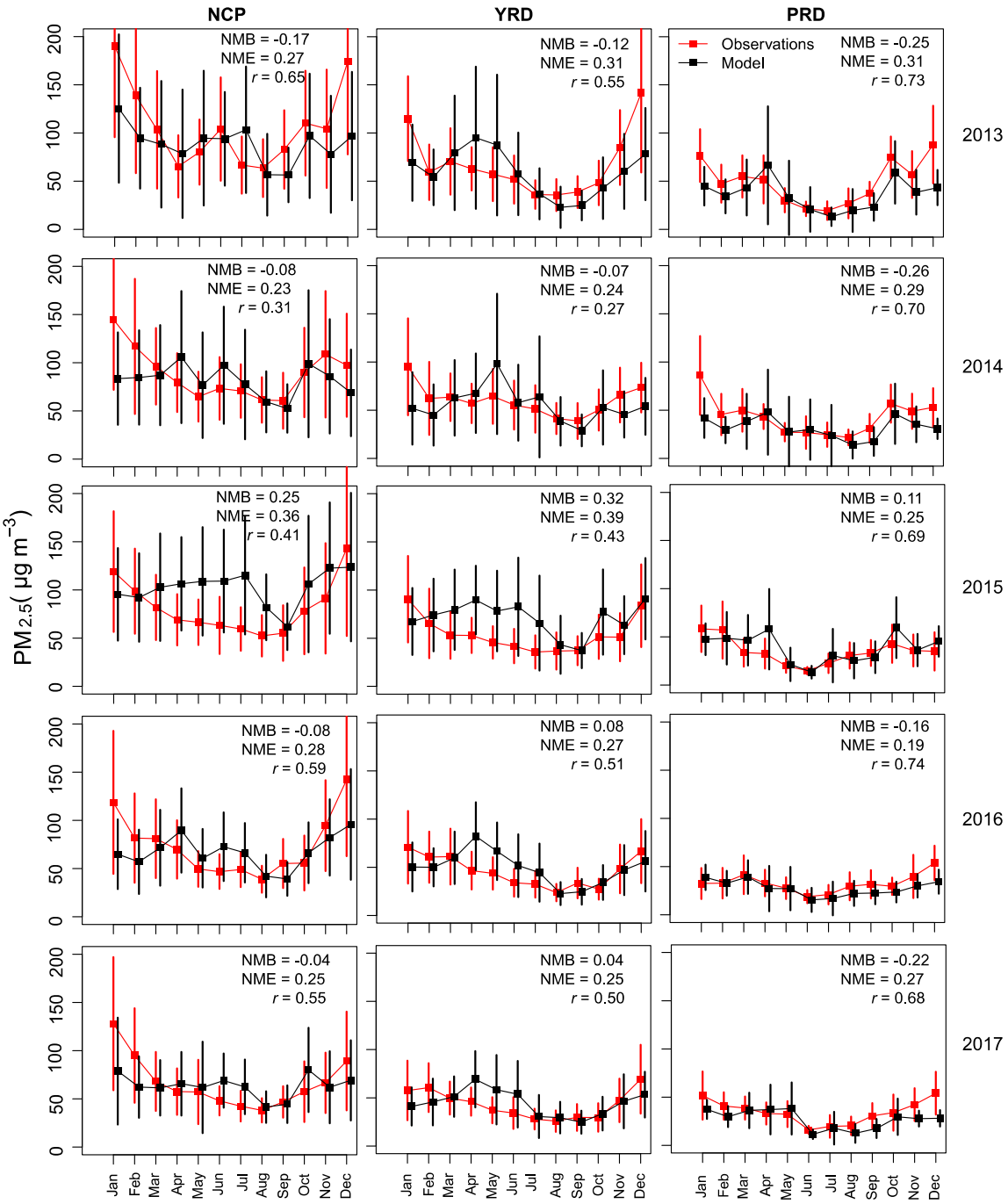

Figure S4. Observed (red line) and GEOS-Chem simulated (BASE, black line) monthly mean surface PM2.5 concentrations (μg m-3) in NCP, YRD and PRD in 2013–2017.

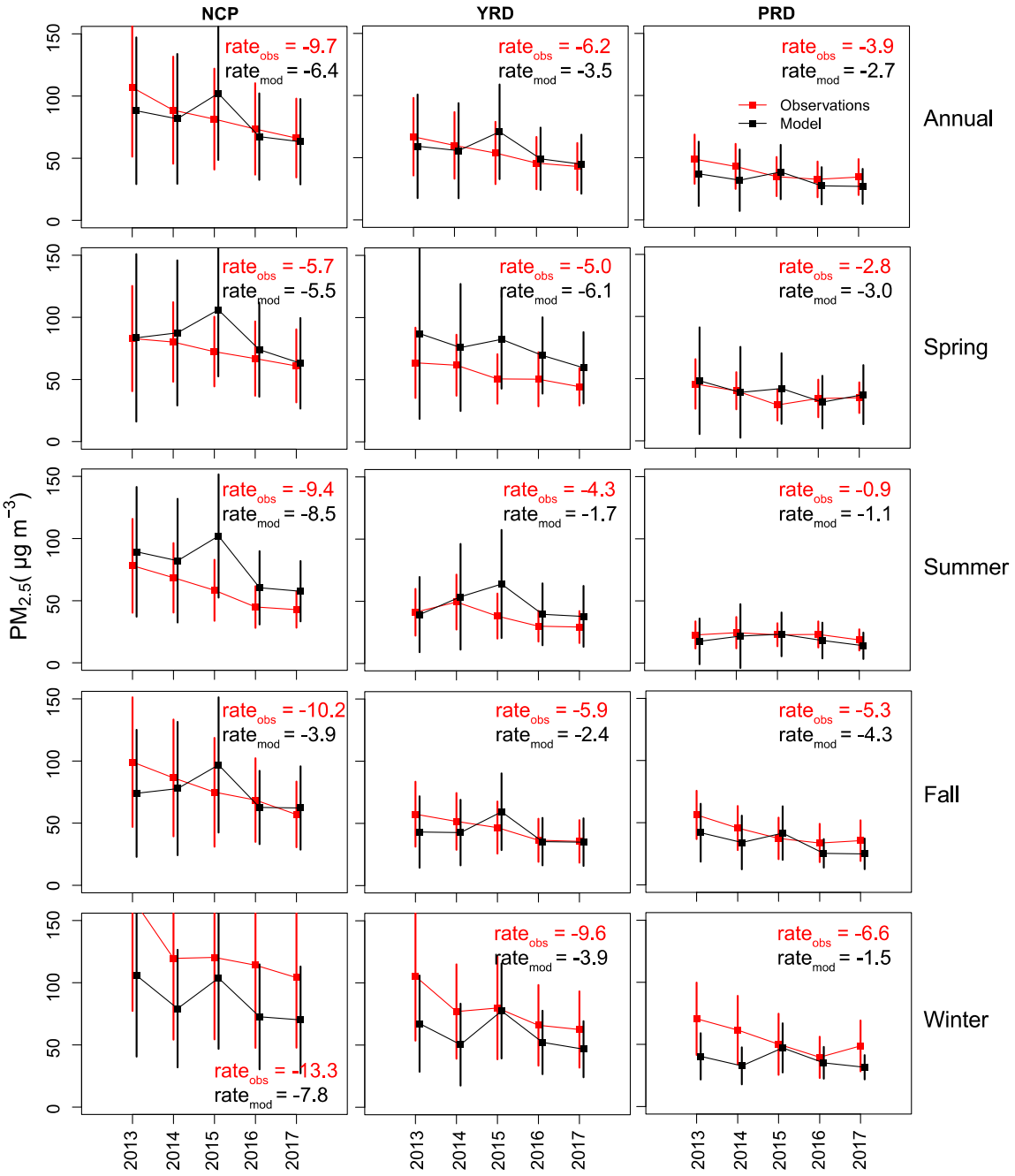

Figure S5: Observed (red line) and GEOS-Chem simulated (BASE, black line) annual and seasonal mean surface $PM_{2.5}$ concentrations (μg m^{-3}) in NCP, YRD and PRD in 2013–2017. The vertical lines are standard deviations of daily means in each season in each year.

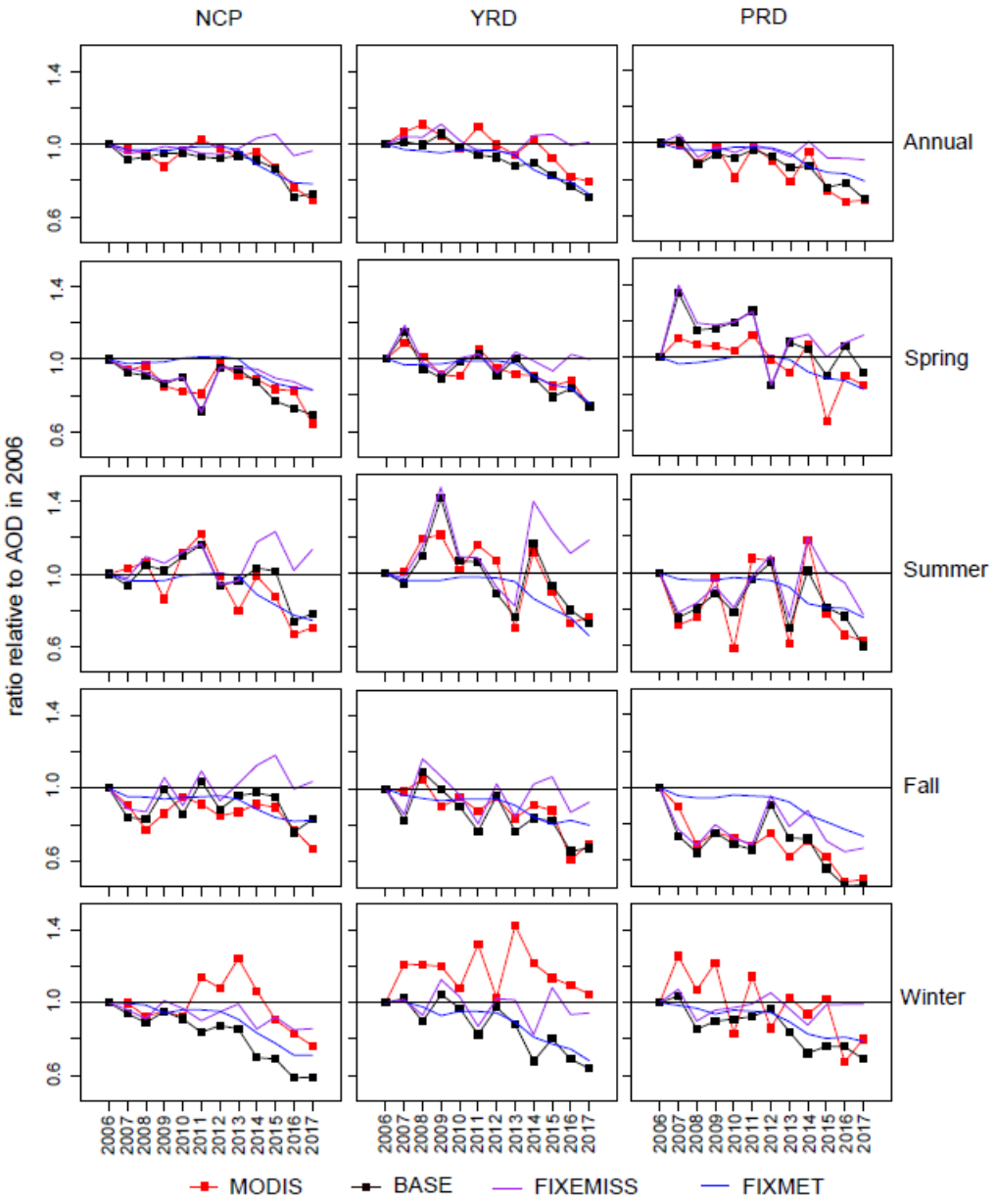

Figure S6: Ratio of annual and seasonal mean AOD relative to their values in 2006 from MODIS (red line) and GEOS-Chem simulations in 2006–2017. Three experiments are shown: varying meteorology and varying emissions (BASE, black line), varying meteorological fields with fixed emissions in 2006 (FIXEMISS, purple line), varying emissions with meteorological fields fixed in 2009 (FIXMET, blue line). See text for details.

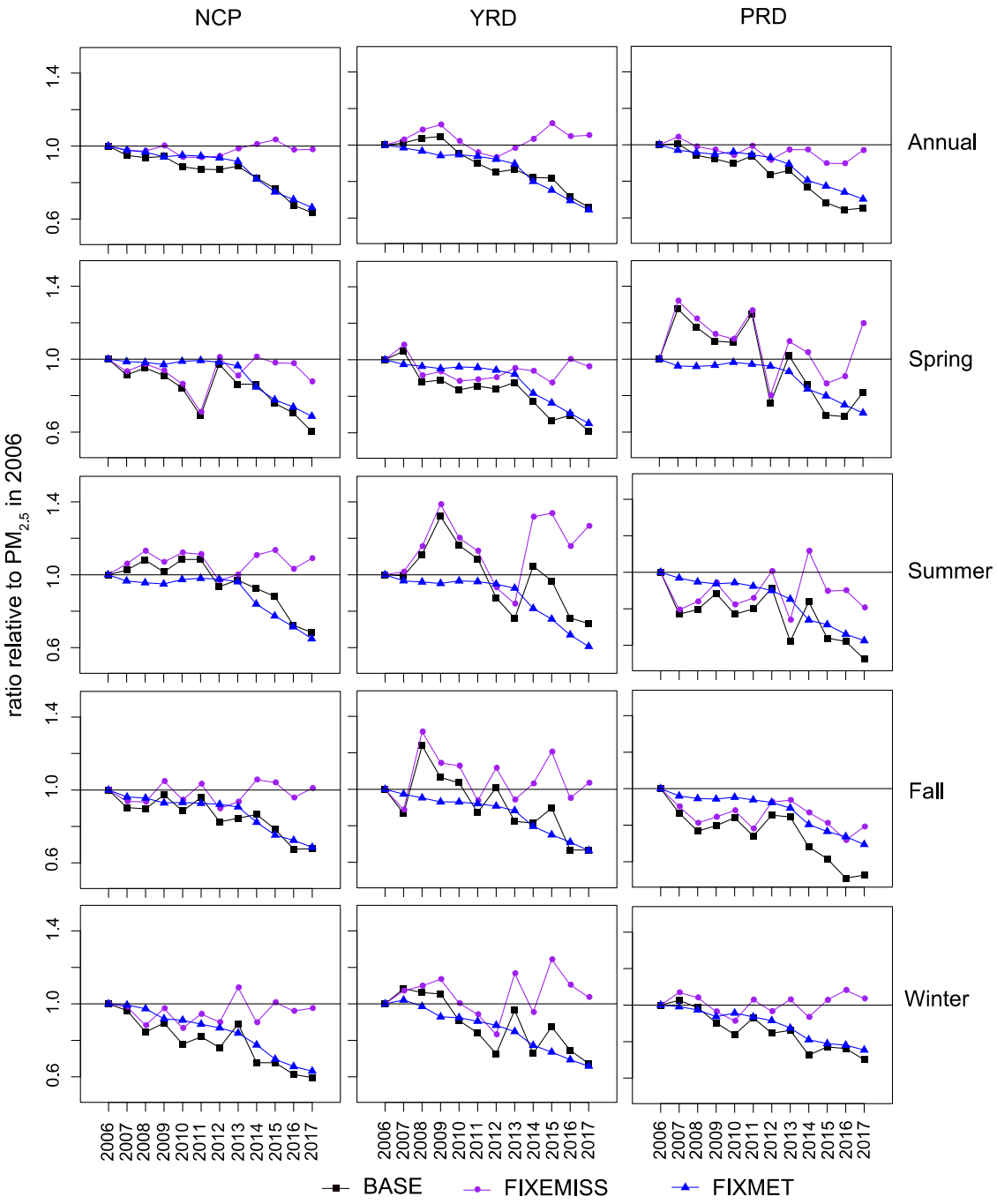

Figure S7: Similar as Figure S6, but for surface $PM_{2.5}$.

Table S1: Statistics of MODIS observed and GEOS-Chem simulated AOD compared to SONET AOD observations at 16 sites.

Site	Type	Region	MODIS			GEOS-Chem BASE		
			r [1]	RMSE [2]	RMSE/ AOD_{SONET} [3] (%)	*r*	RMSE	RMSE/ AOD_{SONET} (%)
Beijing (116.3°E, 40.0°N, 59m)	Urban	NCP	0.71	0.17	24	0.79	0.18	26
Songshan (113.1°E, 34.5°N, 475m)	Moutain	NCP	0.72	0.14	20	0.46	0.30	44
Guangzhou (113.4°E, 23.1°N, 28m)	Coastal/urban	PRD	0.28	0.40	54	0.64	0.39	52
Chengdu (104.0°E, 40.6°N, 510m)	Urban/basin	SCB	-0.31	0.79	88	-0.66	0.64	71
Hefei (117.2°E, 31.9°N, 36m)	Urban	YRD	0.18	0.17	24	0.15	0.27	39
Nanjing (119.0°E, 32.1°N, 52m)	Urban	YRD	0.32	0.13	19	0.07	0.27	39
Zhoushan (122.1°E, 29.9°N, 29m)	Coastal/urban	YRD	0.92	0.13	27	0.65	0.16	32
Shanghai (121.5°E, 31.3°N, 84m)	Coastal/urban	YRD	0.53	0.19	37	0.33	0.21	39
Sanya (109.4°E, 18.3°N, 29m)	Coastal/urban	Other	0.89	0.20	46	0.56	0.33	77
Haikou (110.3°E, 20.0°N, 22m)	Coastal/urban	Other	0.92	0.20	43	0.76	0.31	67
Xi'an (108.9°E, 34.2°N, 389m)	Urban/dust	Other	0.29	0.38	46	-0.34	0.40	49
Harbin (126.6°E, 45.7°N, 223m)	Urban	Other	0.15	0.22	58	0.39	0.13	35
Minqin (100.3°E, 38.8°N, 1589m)	Dust	Other	0.72	0.12	49	0.88	0.13	53
Zhangye (103.0°E, 38.6°N, 1364m)	Dust	Other	0.95	0.11	41	0.61	0.23	82
Kashi (75.9°E, 39.5°N, 1320m)	Dust	Other	0.58	0.38	70	0.52	0.32	57
Lhasa (91.2°E, 29.6°N, 3678m)	Background	Other	-0.70	0.07	88	0.78	0.04	51

[1] Correlation coefficient

[2] Root Mean Square Error, estimated as follows

$$\mathrm{RMSE} = \sqrt{\frac{1}{n}\sum_{i=1}^{n}(\mathrm{AOD}_{\mathrm{MODIS}i} - \mathrm{AOD}_{\mathrm{SONET}i})^2}$$

where n is the number of AOD measurements. In this study, we use monthly mean AOD measurements, thus n is 12. $AOD_{MODIS}i$ and $AOD_{SONET}i$ are mean AOD from MODIS and SONET in month i at one site.

[3] The ratio of RMSE to annual mean AOD from SONET sites

Table S2: List of abbreviations

Acronym	Full term
AOD	Aerosol optical depth
BC	Black carbon
EASM	East Asian summer monsoon
EAWM	East Asian winter monsoon
MERRA-2	Modern-Era Retrospective analysis for Research and Application, Version 2
NCP	North China Plain
O	Vertical air movement
OC	Organic carbon
$PM_{2.5}$	Fine particle with diameter of 2.5 μm and smaller
PRD	Pearl River Delta
PV	Potential vorticity
PS	Pressure at surface
PBLH	Planetary boundary layer height
PREC	Precipitation
RH	Relative humidity
SLP	Sea level pressure
T	Temperature
TROPPT	Tropopause pressure
U	Zonal wind speed
V	Meridional wind speed
WPSTH	West Pacific Sub-Tropical High system
YRD	Yangtze River Delta

References

1. Li, Z.Q.; Xu, H.; Li, K.T.; Li, D.H.; Xie, Y.S.; Li, L.; Zhang, Y.; Gu, X.F.; Zhao, W.; Tian, Q.J.; et al. Comprehensive Study of Optical, Physical, Chemical, and Radiative Properties of Total Columnar Atmospheric Aerosols over China: An Overview of Sun–Sky Radiometer Observation Network (SONET) Measurements. *Bull. Am. Meteorol. Soc.* **2018**, *99*, 739–755. https://doi.org/10.1175/bams-d-17-0133.1.
2. Eck, T.F.; Holben, B.N.; Reid, J.S.; Dubovik, O.; Smirnov, A.; O'Neill, N.T.; Slutsker, I.; Kinne, S. Wavelength dependence of the optical depth of biomass burning, urban, and desert dust aerosols. *J. Geophys. Res.* **1999**, *104*, 31333–31349. https://doi.org/10.1029/1999JD900923.
3. Cheng, T.; Chen, H.; Gu, X.; Yu, T.; Guo, J.; Guo, H. The inter-comparison of MODIS, MISR and GOCART aerosol products against AERONET data over China. *J. Quant. Spectrosc. Radiat. Transf.* **2012**, *113*, 2135–2145. https://doi.org/10.1016/j.jqsrt.2012.06.016.
4. Bilal, M.; Nazeer, M.; Nichol, J.; Qiu, Z.; Wang, L.; Bleiweiss, M.; Shen, X.; Campbell, J.; Lolli, S. Evaluation of Terra-MODIS C6 and C6.1 Aerosol Products against Beijing, XiangHe, and Xinglong AERONET Sites in China during 2004–2014. *Remote Sens.* **2019**, *11*, 486–501. https://doi.org/10.3390/rs11050486.
5. He, Q.; Li, C.; Tang, X.; Li, H.; Geng, F.; Wu, Y. Validation of MODIS derived aerosol optical depth over the Yangtze River Delta in China. *Remote Sens. Environ.* **2010**, *114*, 1649–1661. https://doi.org/10.1016/j.rse.2010.02.015.
6. Li, Z.; Zhao, X.; Kahn, R.; Mishchenko, M.; Remer, L.; Lee, K.; Wang, M.; Laszlo, I.; Nakajima, T.; Maring, H. Uncertainties in satellite remote sensing of aerosols and impact on monitoring its long-term trend: A review and perspective. *Ann. Geophys*. **2009**, *27*, 2755–2770. https://doi.org/10.5194/angeo-27-2755-2009.
7. Harrison, D.; Maggs, R.; Booker, J. *UK Equivalence Programme for Monitoring of Particulate Matter*; BV/AQ/AD202209/DH/2396; Bureau Veritas: London, UK, 2006.
8. Li, S.; Yu, C.; Chen, L.; Tao, J.; Letu, H.; Ge, W.; Si, Y.; Liu, Y. Inter-comparison of model-simulated and satellite-retrieved componential aerosol optical depths in China. *Atmos. Environ.* **2016**, *141*, 320–332. https://doi.org/10.1016/j.atmosenv.2016.06.075.
9. Li, S.; Zhang, L.; Cai, K.; Ge, W.; Zhang, X. Comparisons of the vertical distributions of aerosols in the CALIPSO and GEOS-Chem datasets in China. *Atmos. Environ. X* **2019**, *3*, 100036. https://doi.org/10.1016/j.aeaoa.2019.100036.
10. Wang, Q.; Jacob, D.J.; Spackman, J.R.; Perring, A.E.; Schwarz, J.P.; Moteki, N.; Marais, E.A.; Ge, C.; Wang, J.; Barrett, S.R.H. Global budget and radiative forcing of black carbon aerosol: Constraints from pole-to-pole (HIPPO) observations across the Pacific. *J. Geophys. Res. Atmos.* **2014**, *119*, 195–206. https://doi.org/10.1002/2013jd020824.
11. Zhang, L.; Kok, J.F.; Henze, D.K.; Li, Q.; Zhao, C. Improving simulations of fine dust surface concentrations over the western United States by optimizing the particle size distribution. *Geophys. Res. Lett.* **2013**, *40*, 3270–3275. https://doi.org/10.1002/grl.50591.
12. Hammer, M.S.; Martin, R.V.; van Donkelaar, A.; Buchard, V.; Torres, O.; Ridley, D.A.; Spurr, R.J.D. Interpreting the ultraviolet aerosol index observed with the OMI satellite instrument to understand absorption by organic aerosols: Implications for atmospheric oxidation and direct radiative effects. *Atmos. Chem. Phys.* **2016**, *16*, 2507–2523. https://doi.org/10.5194/acp-16-2507-2016.
13. Fairlie, T.D.; Jacob, D.J.; Dibb, J.E.; Alexander, B.; Avery, M.A.; van Donkelaar, A.; Zhang, L. Impact of mineral dust on nitrate, sulfate, and ozone in transpacific Asian pollution plumes. *Atmos. Chem. Phys.* **2010**, *10*, 3999–4012. https://doi.org/10.5194/acp-10-3999-2010.
14. Li, S.; Chen, L.; Fan, M.; Tao, J.; Wang, Z.; Yu, C.; Si, Y.; Letu, H.; Liu, Y. Estimation of GEOS-Chem and GOCART Simulated Aerosol Profiles Using CALIPSO Observations over the Contiguous United States. *Aerosol Air Qual. Res.* **2017**, *16*, 3256–3265. https://doi.org/10.4209/aaqr.2015.03.0173.
15. Sogacheva, L.; Rodriguez, E.; Kolmonen, P.; Virtanen, T.H.; Saponaro, G.; de Leeuw, G.; Georgoulias, A.K.; Alexandri, G.; Kourtidis, K.; van der A, R.J. Spatial and seasonal variations of aerosols over China from two decades of multi-satellite observations-Part 2: AOD time series for 1995–2017 combined from ATSR ADV and MODIS C6.1 and AOD tendency estimations. *Atmos. Chem. Phys.* **2018**, *18*, 16631–16652. https://doi.org/10.5194/acp-18-16631-2018.